Applied Materials Today 23 (2021) 101052

Contents lists available at ScienceDirect

Applied Materials Today

journal homepage: www.elsevier.com/locate/apmt

Ultrabroadband light absorbing Fe/polymer flexible metamaterial for soft opto-mechanical devices

Pau Güell-Grau [a,b], Francesc Pi [c], Rosa Villa [a,d], Josep Nogués [b,e], Mar Alvarez [a,d,*], Borja Sepúlveda [b,*]

[a] Instituto de Microelectrónica de Barcelona (IMB-CNM, CSIC), Campus UAB, Bellaterra 08193, Barcelona, Spain
[b] Catalan Institute of Nanoscience and Nanotechnology (ICN2), CSIC and BIST, Campus UAB, Bellaterra 08193, Barcelona, Spain
[c] Departament de Física, Facultat de Ciències, Universitat Autònoma de Barcelona, Bellaterra 08193, Barcelona, Spain
[d] Networking Research Centre on Bioengineering, Biomaterials and Nanomedicine (CIBER-BBN), Spain
[e] ICREA, Pg. Lluís Companys 23, 08010 Barcelona, Spain

ARTICLE INFO

Article history:
Received 19 March 2021
Revised 16 April 2021
Accepted 22 April 2021

Keywords:
Ultrabroadband absorption
Soft metamaterials
Highly-damped plasmonics
Iron nanostructures
Optomechanical devices

ABSTRACT

Ultrabroadband light absorbers are attracting increasing interest for applications in energy harvesting, photodetection, self-regulated devices or soft robotics. However, current absorbers show detrimental insufficient absorption spectral range, or light angle and polarization dependence. Here we show that the unexplored optical properties of highly-damped plasmonic materials combined with the infrared absorption of thin polymer films enable developing ultrabroadband light-absorbing soft metamaterials. The developed metamaterial, composed of a nanostructured Fe layer mechanically coupled to a thin polydimethylsiloxane (PDMS) film, shows unprecedented ultrabroadband and angle-independent optical absorption (averaging 84% within 300–18000 nm). The excellent photothermal efficiency and large thermal-expansion mismatch of the metamaterial is efficiently transformed into large mechanical deflections, which we exploit to show an artificial iris that self-regulates the transmitted light power from the ultraviolet to the long-wave infrared, an untethered light-controlled mechanical gripper and a light-triggered electrical switch.

1. Introduction

Efficient broadband light absorption is crucial for many relevant photonic devices, such as solar cells [1,2], photodetectors [3,4] or soft-actuators [5]. As their performance depends on the ability to collect and convert light into other types of energies, novel concepts are being studied to maximize the absorption spectral window [6]. Recent broadband absorbing metamaterials include microstructures with resonators [7,8], plasmonic nano-composites [9,10], or graphene-based metamaterials [11]. Plasmonic nanostructures are particularly interesting to achieve strong absorbing metamaterials due to their easily tunable optical properties. However, highly efficient light absorption is restricted to small particles compared to the light wavelength and to the excitation of localized surface plasmon resonances in a narrow spectral band. Although resonances can be tuned by size increasing, this imposes a large scattering/absorption ratio enhancement in most plasmonic materials. This effect is more noticeable for resonances in the infrared (IR), where these materials behave as near perfect conductors with minimal radiation penetration, thereby drastically increasing the reflected and scattered light. To expand the absorption range of plasmonic materials, the use of plasmonic nanoparticles of different sizes [12–15], their combination with dielectric layers [16,17], or the nanometric control of their near-field interaction [18,19] have been proposed. Additionally, apart from conventional photonic/plasmonic materials, there are other materials, like transition metals, which have been barely explored for photonic applications and/or efficient light absorption, as is the case of metallic iron (Fe). Fe shows a negative real part of the dielectric constant from the ultraviolet (UV) to the far-IR, which is an essential condition for the generation of plasmonic resonances. However, its imaginary part is much larger than in classical plasmonic materials. This results in a large plasmonic damping, which prevents the generation of sharp resonances, hampering its application in typical plasmonic applica-

* Corresponding authors.
E-mail addresses: mar.alvarez@csic.es (M. Alvarez), borja.sepulveda@icn2.cat (B. Sepúlveda).

https://doi.org/10.1016/j.apmt.2021.101052

tions such as refractometric sensors or biosensors [20], or the generation of enhanced electromagnetic fields at the nanostructures edges. However, these broad resonances make Fe ideal for broadband absorption applications. Fe enables a deeper electromagnetic field penetration inside the nanostructures, thus minimizing light reflectance/scattering. This feature is particularly appealing to combine nanostructured-Fe absorption with highly absorbing materials in the far-IR, like flexible polymers, whose enhanced absorption bands in the midwave-IR–longwave-IR (MWIR-LWIR) range have been rarely exploited for practical photonic applications. Incorporating ultrabroadband light absorption into polymers is particularly appealing for developing light-controlled soft actuators, as a base for innovative applications in soft robotics [21–25], energy harvesters [26–28] or self-regulated devices [29–31]. Importantly, these applications demand strong ultrabroadband light absorption, incident light angle and polarization independence (due to the large mechanical deflections), and high compliance between the metal and the flexible polymer substrate. However, all the soft actuators reported to date fail in at least one of these requirements.

Here we show that the highly-damped plasmons in nanostructured Fe films (hexagonal close-packaged Fe semi-shells) exhibit extremely efficient broadband absorption in the UV–near-infrared (UV-NIR) with minimal reflectance in the MWIR-LWIR. This, combined with flexible polydimethylsiloxane (PDMS) films showing enhanced light absorption in the MWIR-LWIR, enables developing soft metamaterials with an unprecedented ultrabroadband absorption range. This inexpensive novel metamaterial shows an angle-independent and efficient ultrabroadband optical absorption range (average 84% within 300-18000 nm), which results in an excellent photothermal conversion efficiency. Due to the large thermal-expansion-coefficient mismatch between both materials, the photoinduced temperature increase is efficiently transformed into large mechanical deflections. We exploit these features to demonstrate three soft photo-thermo-mechanical devices: (i) a power-free, ultrabroadband, self-regulated artificial iris that adjusts its aperture to the light intensity (from UV to far-IR), thus mimicking a natural iris or acting as a self-regulated radiation protector; (ii) an optically-controlled mechanical gripper, enabling picking, transporting and releasing cargos, and (iii) an untethered optically-triggered electrical switch.

2. Materials and methods

2.1. Simulations

The finite-difference time-domain (FDTD) simulations were carried out by the Lumerical Software, having a mesh of 2 nm in the region containing the metal structures. For the forward/back-scattering simulation, a 900 $\times$ 900 nm^2 detector plane was placed 100 nm before/after the semi-shell structure. The FDTD calculation volume is a cube of 1 µm edge.

2.2. Fabrication

Firstly, the PDMS thin layer was obtained by spin-coating liquid PDMS (*Sylgard 184*) at 1000 rpm for 90 seconds on a thick (5 mm) PDMS substrate, previously coated with *(Tridecafluoro-1,1,2,2-tetrahydrooctyl)trichlorosilane (97%, ABCR),* and curing it at 80°C for 30 minutes. In parallel, to obtain the nanostructured metal layers, a hexagonal close-packed colloidal self-assembly of polystyrene nanospheres (diameter 200/300/500 nm) (*Life Technologies*) on a silicon substrate is prepared. To do the assembly, the close-packed monolayer of spheres is first formed at the air/water interface that is on the immersed silicon wafer. Once the monolayer is fully formed, the water is drained and the layer is deposited on the silicon substrate. After drying, the metal film (gold/iron) is deposited (40/80 nm) by electron beam physical vapor deposition (*UNIVEX 450, Leybold*). The nanostructured metal films were then transferred to the cured PDMS by contact transfer printing. A laser cutter (*Epilog Mini 24, Epilog Laser*) was used to define and cut the self-suspended structures into the desired geometry and dimensions. The structures were then released from the substrate by using a 0.5 mm thick poly(methyl methacrylate) with double-sided pressure-sensitive adhesive as base support.

2.3. Morphological characterization

The morphology of the nanostructured metal films on PDMS was examined by Scanning Electron Microscopy (*Quanta FEG650, FEI (ThermoFisher)*).

2.4. Optical characterization

The UV-Visible-NIR transmission spectrometry was carried out using a fiber-coupled halogen light source (HL2000, Ocean Optics), with an optical fiber (*Ø = 400 µm, NA = 0.5; M45L01, Thorlabs*) and an aspheric lens (*Thorlabs*) to collimate the light. The optical spectra were recorded by two spectrometers for the UV-visible (*Flame, Ocean Optics®*) and near-infrared (*NIRQuest, Ocean Optics*) ranges. The UV-Visible-NIR reflection spectrometry was carried out using a bifurcated optical fiber bundle (*M25L01, Thorlabs*), a silver mirror as a reference (PF10-03-P01, *Thorlabs*) and the same light source and spectrometers as for transmission. Infrared spectrometry was carried out by a Fourier Transform Infrared Spectrometer (FTIR) (*Bruker Vertex80*), using a gold film as a reference for reflection and a KBr (FT-IR grade, *Sigma Aldrich*) sample substrate as a reference for transmission.

2.5. Photothermal characterization

Temperature monitoring of the sample was carried out using a non-contact infrared thermometer (*MLX90614, Melexis*) and a computer with Labview data acquisition software. The infrared sensing characterization was carried out using a white light LED (MWWHLP1, Thorlabs), a NIR laser diode with emission wavelength at 808 nm (B1-808-1500-15A, Sheaumann) and another laser with emission at 1470 nm (QSM-1470-3, QPhotonics). A germanium filter (WG90530-G, *Thorlabs*) was used to block the interferences at the infrared thermometer coming from the infrared light sources. Sunlight photothermal characterization was calibrated using an optical power meter (S310C, PM100D, *Thorlabs)* and measured using an infrared thermal camera (*FLIR*).

2.6. Optomechanical characterization

The angle change of the cantilever and aperture change of the artificial iris was recorded using a conventional USB camera (*DinoLite*) and *DinoCapture* as the image capture software. The light sources were the same as for the photothermal characterization. The IR thermal emission was produced by heating a PDMS and aluminum sample using a single stage TEC Element (TECD6, *Thorlabs*). The transmitted power was measured using two different optical power meters for visible-NIR light (S310C, PM100D, *Thorlabs)* and for thermal IR (S401C, *Thorlabs*).

3. Results and discussion

To highlight the key differences between classical plasmonic absorbers and highly-damped plasmonic materials for ultrabroadband absorption applications, we compare the scattering and absorption cross sections of identical gold (Au) and Fe structures

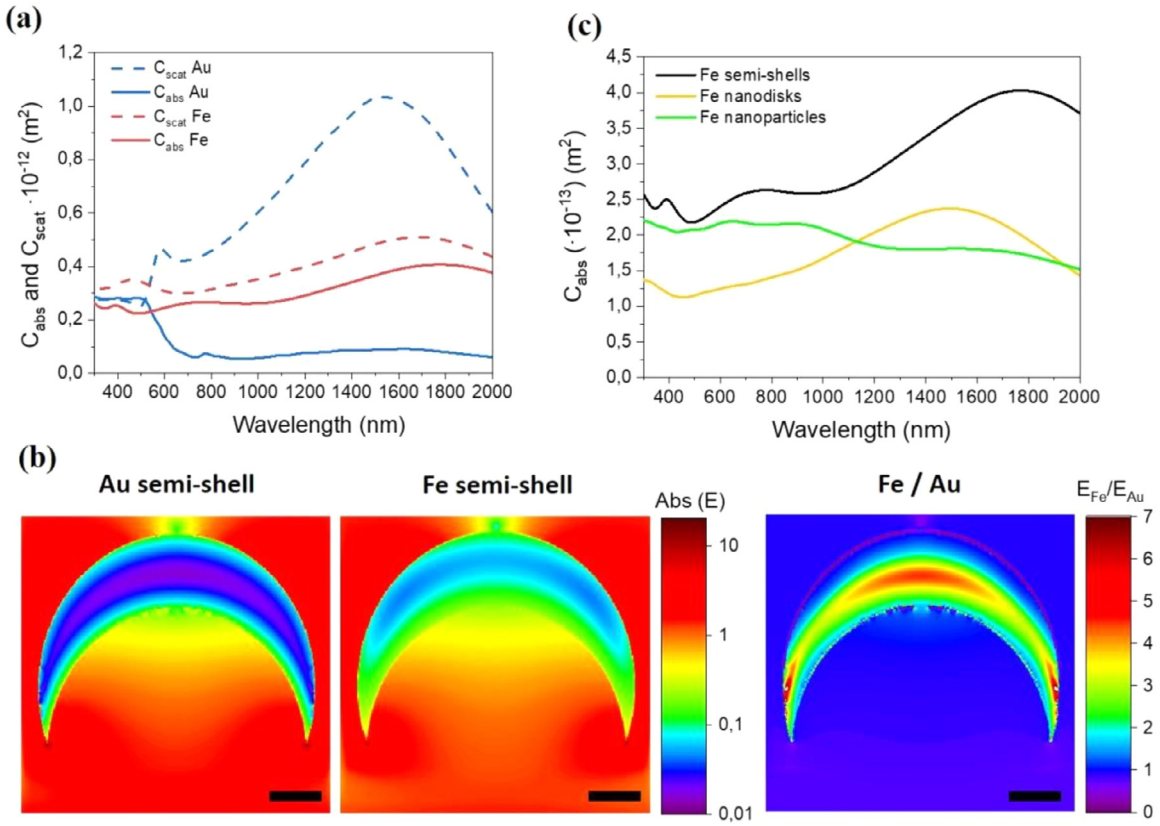

Fig. 1. (a) FDTD simulations comparing the scattering (C_{scat}) and absorption (C_{abs}) cross-sections for 500 nm diameter Au and Fe semi-shell structures. (b) Electric field distribution in the central plane for Au (left) and Fe (center) semi-shells and the ratio of the electric fields observed in each structure (right), evidencing the much larger light penetration inside the Fe structure. Scale-bar = 100 nm. (c) Comparison of the C_{abs} for Fe structures of different shapes and constant size (diameter = 500 nm).

by finite-difference time-domain (FDTD) simulations. As a rule of thumb, to achieve strong absorption, the absorption/scattering ratio of the structures should be maximized, whereas very broad/flat spectra are required to reach the ultrabroadband absorption. From the FDTD calculations, we observe that Fe semi-shell structures of 500 nm diameter exhibit approximately 7-fold larger absorption cross-section compared to their

Au A Au counterparts (Fig. 1a). Moreover, the large scattering observed in the Au structures is dramatically reduced (between 2 and 3-fold) in the Fe semi-shell.

Overall, the absorption/scattering ratio of Fe semi-shells can be up to 25-fold larger than Au semi-shells in the NIR, thus highlighting their potential to achieve intense light absorption efficiency. The reason behind this stark difference is the much higher penetration of the light inside the highly damped plasmonic Fe semi-shell compared to the Au structures, as shown by the electric field distribution around and inside the metal structures, which is almost 6-fold higher at the central thickest part of the Fe metal structure (Fig. 1b). The larger light penetration in Fe is endowed by both the lower absolute value of the real part of the dielectric constant and the much higher imaginary part (up to 20-fold larger at 800 nm wavelength compared to Au). This large difference in the absorption/scattering ratio is also clearly observed in other common plasmonic materials, like Ag and Al semi-shells (Fig. S1a).

Interestingly, the Fe semi-shells also enable stronger absorption in a much broader spectral range (from the UV to the NIR), even covering wavelengths shorter than the size of the nanostructures. In addition to the scattering reduction compared to Au, the FDTD simulations show that the forward scattering is favored with respect to the back scattering (Fig. S1b). This is essential to allow the MWIR and LWIR radiation (that is not so efficiently absorbed by the Fe structures) to be transmitted and totally absorbed by another material, such as a thin flexible polymer layer with strong absorption bands in this range. Notably, the structure geometry also plays a major role to maximize the spectral absorption range, where other more common geometries, such as spheres or discs, show substantially lower absorption bands (Fig. 1c). Finally, it is worth highlighting that this type of highly damped plasmonic Fe semi-shell structures can be easily obtained by colloidal self-assembly and highly directional Fe evaporation. In addition, the inherent potential to adjust the colloidal size and separation distance between self-assembled structures can also be exploited to attain even broader absorption bands. The combination of self-assembled Fe semi-shells with a polymer film gives rise to an absorbing metamaterial enabling the efficient light absorption in the whole UV to IR regime, which otherwise would be almost totally reflected by a continuous iron film.

Considering the previous theoretical results, the fabrication process of the nanostructured-Fe/PDMS metamaterial is based on a scalable combination of colloidal self-assembly, physical vapor deposition and polymer casting (Fig. 2a). The nanostructured-Fe film is prepared by the hexagonal close-packed self-assembly of a monolayer of polystyrene (PS) nanospheres (500 nm diameter) followed by the electron beam deposition of the Fe layer (80 nm), leading to a “semi-shell” structure [32,33]. The nanostructured-Fe film is mechanically coupled to the PDMS layer (50 μm) by transfer printing (Fig. 2b). Once the metamaterial is fabricated, the generation of the opto-mechanical structures for soft actuation applications is performed by defining the desired geometries by laser writing and releasing them from the substrate, thus yielding free-standing structures. Note that the released structures have an initial curvature due to the generated residual stress during the re-

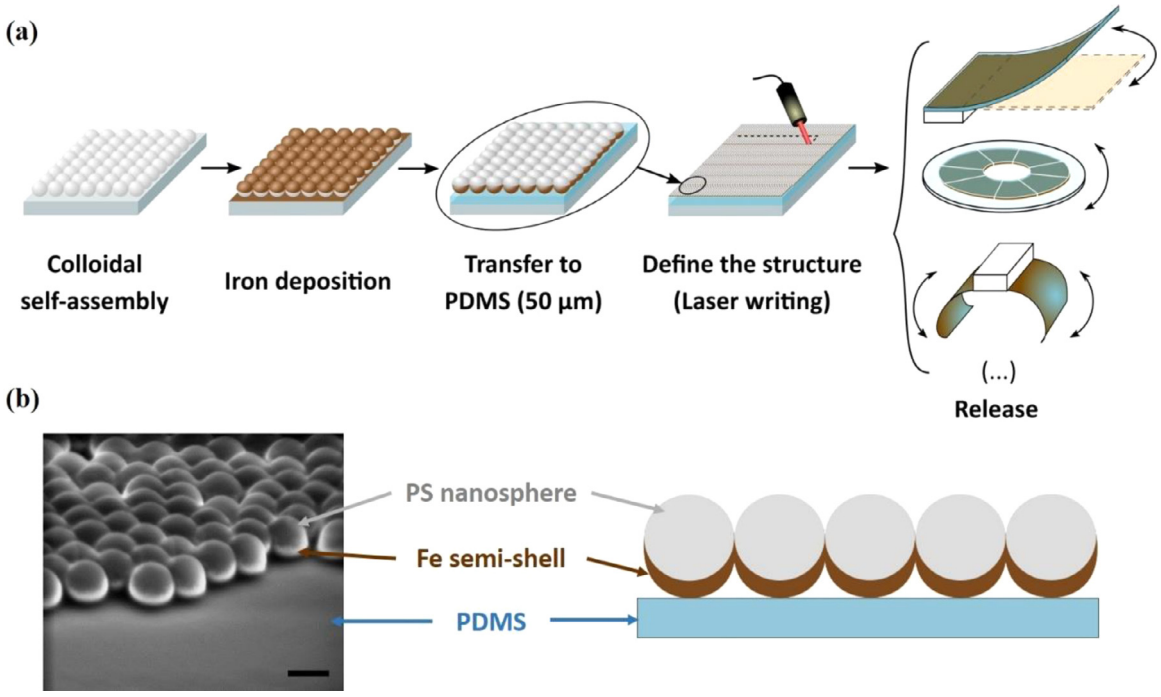

Fig. 2. (a) Schematic of the fabrication steps of the Fe/PDMS metamaterial. (b) SEM image and schematic representation of the nanostructured-Fe layer in contact to the PDMS layer (scale-bar = 500 nm).

leasing step. It is worth emphasizing that this fabrication process is straightforward, fast, inexpensive and easily scalable.

In agreement with the FDTD simulations, the experimental characterization of the Fe/PDMS metamaterial demonstrated a very high optical absorption of the nanostructured-Fe layer within the Ultraviolet–Visible–Near Infrared (UV-vis- NIR) ranges (300 – 2000 nm) where the PDMS is transparent [34] (Fig. 3a). Moreover, the nanostructured-Fe layer minimizes the reflectance in the MWIR and LWIR infrared regions (2000 - 18000 nm) (Fig. S2), thereby enabling the transmission and posterior absorption of these wavelengths by the PDMS layer, which is an efficient absorber in this range (Fig. 3b). The synergistic combination of the optical properties of both layers results in an outstanding ultrabroadband absorption range from the UV to the LWIR, 300 – 18000 nm, with an average 84% absorption (Fig. 3a,b). In comparison with previously reported strong (>80%) absorbers, the Fe/PDMS metamaterial shows a competitive absorption (from 75% to 94%) within a much broader wavelength range than any other reported absorber within the UV to LWIR range (see Table S1) [7,9–11,18,22,35,36-43]. In contrast, the Au/PDMS metamaterial showed substantially weaker absorption (Fig. 3a,b) because of the increased reflection of the nanostructured-Au (Fig. S2a,b), as suggested by the FDTD simulations. The different performance between both metals is due to the highly damped plasmonic behavior of Fe, which provides deeper electromagnetic field penetration inside the metal to maximize the absorption in the UV-vis-NIR (as previously shown in Fig. 1b), and the transmittance in the MWIR and LWIR. Oppositely, the nanostructured-Au layer behaves as a near-perfect conductor in the NIR-LWIR, thereby enhancing the reflectance and decreasing even further the absorption efficiency. The superior absorption efficiency in the Fe/PDMS with respect to the Au/PDMS metamaterial was also observed for semi-shells of other diameters and different metal thicknesses (Fig. S3). Note that by selecting the appropriate thickness of the Fe layer or the diameter of the nanostructures in the nanostructured-Fe layer, the minimum absorption of the metamaterial in the UV – NIR could be further enhanced to above 80% (Fig. S3b).

The photothermal conversion efficiency, $\eta = dT/dI$ (where T is temperature and I is the light irradiance), was determined by irradiating the metamaterials with four different light sources: white-LED (410–700 nm), 808 nm and 1470 nm lasers, and natural sunlight. The change of temperature was found to be proportional to the light intensity for all the light sources (Fig. 3c). Moreover, the photothermal conversion efficiency of the Fe/PDMS-metamaterial did not significantly differ for any light source, which is in accordance with its nearly-flat broadband absorption. Importantly, the η of the Fe/PDMS-metamaterial exhibited minimal dependence on the light incidence angle, which is critical to provide a linear photo-thermo-mechanical response in structures with high curvatures, thus overcoming the angular limitation inherent to other absorbers [34,44]. As expected from the absorption spectra, the Fe/PDMS-metamaterial showed substantially higher η (ca. 2-fold) than the analogous Au/PDMS-metamaterial at normal incidence. Moreover, the nanostructured-Au layer presented strong angular dependence due to the diffraction-coupling to surface-plasmon-polaritons.

The optomechanical response was assessed in Fe/PDMS metamaterial cantilevers (Fig. 4a) by measuring the curvature changes as a function of the light intensity (Fig. 4b). In bimorph structures the curvature change is produced by the thermal strain $\Delta\varepsilon$ generated by the light-induced temperature increase ΔT, $\Delta\varepsilon = (\alpha_{PDMS} - \alpha_{Fe})\Delta T$, where α_{PDMS} and α_{Fe} are the thermal expansion coefficients of PDMS and Fe, respectively. Since the PDMS layer thickness is much larger than the Fe layer ($t_{PDMS} >> t_{Fe}$), the equation of the curvature ($1/r$) change can be simplified to [22]:

$$\frac{1}{r} = \frac{(\alpha_{\mathrm{PDMS}} - \alpha_{\mathrm{Fe}})\Delta T}{\frac{E_{\mathrm{PDMS}} t_{\mathrm{PDMS}}{}^2}{6E_{\mathrm{Fe}} t_{\mathrm{Fe}}} + \frac{2t_{\mathrm{PDMS}}}{3}} \quad (1)$$

Where r is the curvature radius (Fig. 4b, inset), and E_{PDMS} and E_{Fe} are the Young's-modulus of the PDMS and nanostructured-Fe layers, respectively.

The parameter "$1/r$" was chosen to quantify the curvature variations and to compare with the literature results, since it is independent of the cantilever length. The cantilever curvature changed

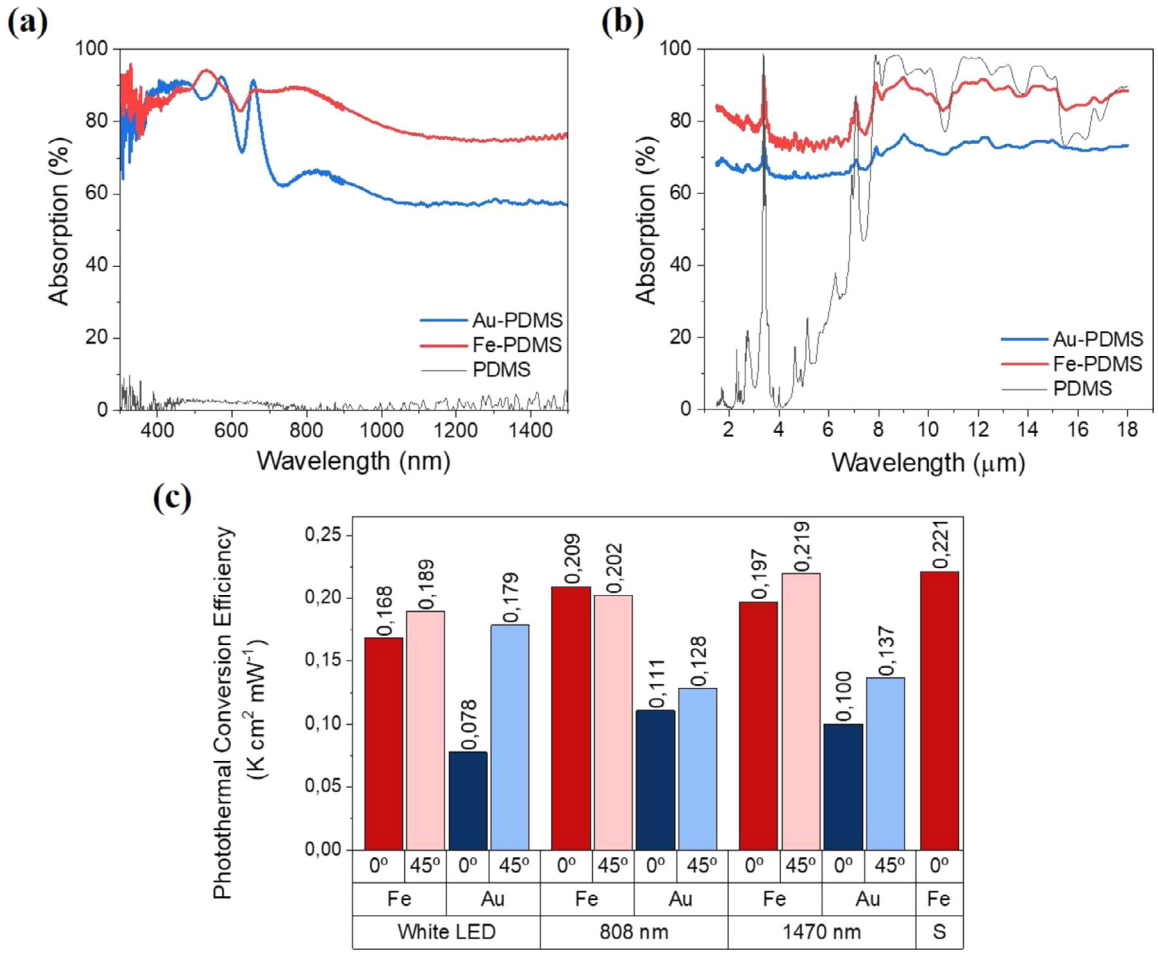

Fig. 3. (a,b) Absorption spectra of the Fe/PDMS- and Au/PDMS- metamaterials (a) in the UV-visible-NIR range, and (b) in the MWIR- LWIR range. (c) Photothermal conversion efficiency of the Fe/PDMS- and Au/PDMS- metamaterials for light sources of different emission wavelengths and incident angles ("S" = natural sunlight).

linearly with the light-induced temperature changes, and therefore with the light intensity, showing a responsivity of 0.012 cm·mW^{-1}. The excellent photo-thermo-mechanical actuation of the Fe/PDMS-metamaterial is achieved by: i) the highly-efficient light absorption in an unprecedentedly broad spectral range to maximize the light-induced temperature changes, and ii) the large thermal expansion coefficient mismatch between both materials ($\alpha_{Fe} = 1.2\times10^{-5}$ K^{-1}, $\alpha_{PDMS} = 3\times10^{-4}$ K^{-1}).

By fitting the experimental curvature to Eq. (1) (assuming $t_{PDMS} = 50$ μm, $t_{Fe} = 80$ nm, $E_{PDMS} = 1.4$ MPa, $\alpha_{Fe} = 1.2\times10^{-5}$ K^{-1}, $\alpha_{PDMS} = 3\times10^{-4}$ K^{-1}), the effective-Young's-modulus of the nanostructured-Fe layer was extracted, yielding 1.2 GPa. This value demonstrates that the nanostructured-Fe layer behaves as a continuous layer but with a substantially lower Young's-modulus than bulk-Fe (100–200 GPa), thereby highlighting its behavior as both optical and mechanical metamaterial.

Compared to other bimorph actuators, the Fe/PDMS metamaterial presents a better responsivity than other actuators of similar thickness (Fig. 4c). Moreover, according to Eq. (1), the opto-mechanical responsivity can be further enhanced by reducing the PDMS thickness [45]. We could demonstrate this ability by reducing the PDMS thickness to 20 μm, which yielded a responsivity increase up to 0.018 cm·mW^{-1}, thus surpassing again the responsivity reported in the literature in that thickness range (Fig. 4c). Compared to the carbon-ink based bimorph actuator, which has the highest reported responsivity, the Fe/PDMS metamaterial exhibits a substantially flatter absorption spectra, showing minimal variations (i.e., less than 15%) from the UV to the LWIR, whereas the carbon ink suffers an absorption decrease of 2.5 orders of magnitude from the blue to 2.6 μm wavelength. Such flatter and higher absorption efficiency enables using a 15-fold thinner iron absorption layer, with respect to the carbon ink layer. The main limitation of the Fe/PDMS metamaterial comes from the difficulty to achieve mechanically stable PDMS layers with thickness below 20 μm, thus limiting the achievable curvature changes from the bimetallic effect, as predicted by Eq. (1).

To exploit the excellent optomechanical responsivity of the Fe/PDMS metamaterial, we explored the application of this metamaterial in three different light-controlled devices. Specifically, we designed, (i) a self-regulated artificial iris, (ii) a light-regulated soft-robotic gripper and iii) an optically-triggered electrical switch.

Firstly, we developed a self-regulated iris mimicking the behavior of the human iris. A power-free, self-regulated iris might be a solution to ophthalmological problems related to the size and dynamics of the pupil/iris, by controlling the amount of light that reaches the retina [56]. In addition, the same design can be used for an automatic light transmission control (i.e., an optical attenuator for light protection) of any source emitting in the 300–18000 nm range. Note that our iris design was geometrically inspired by a previously reported artificial iris based on liquid crystal elastomers (LCE) [30] working in the 400–600 nm range. Using the standard dimensions of a natural iris [57] the device consisted of a circular Fe/PDMS membrane fixed at its outer diameter (11 mm) with an inner circular hole of 3 mm. The circular membrane was divided

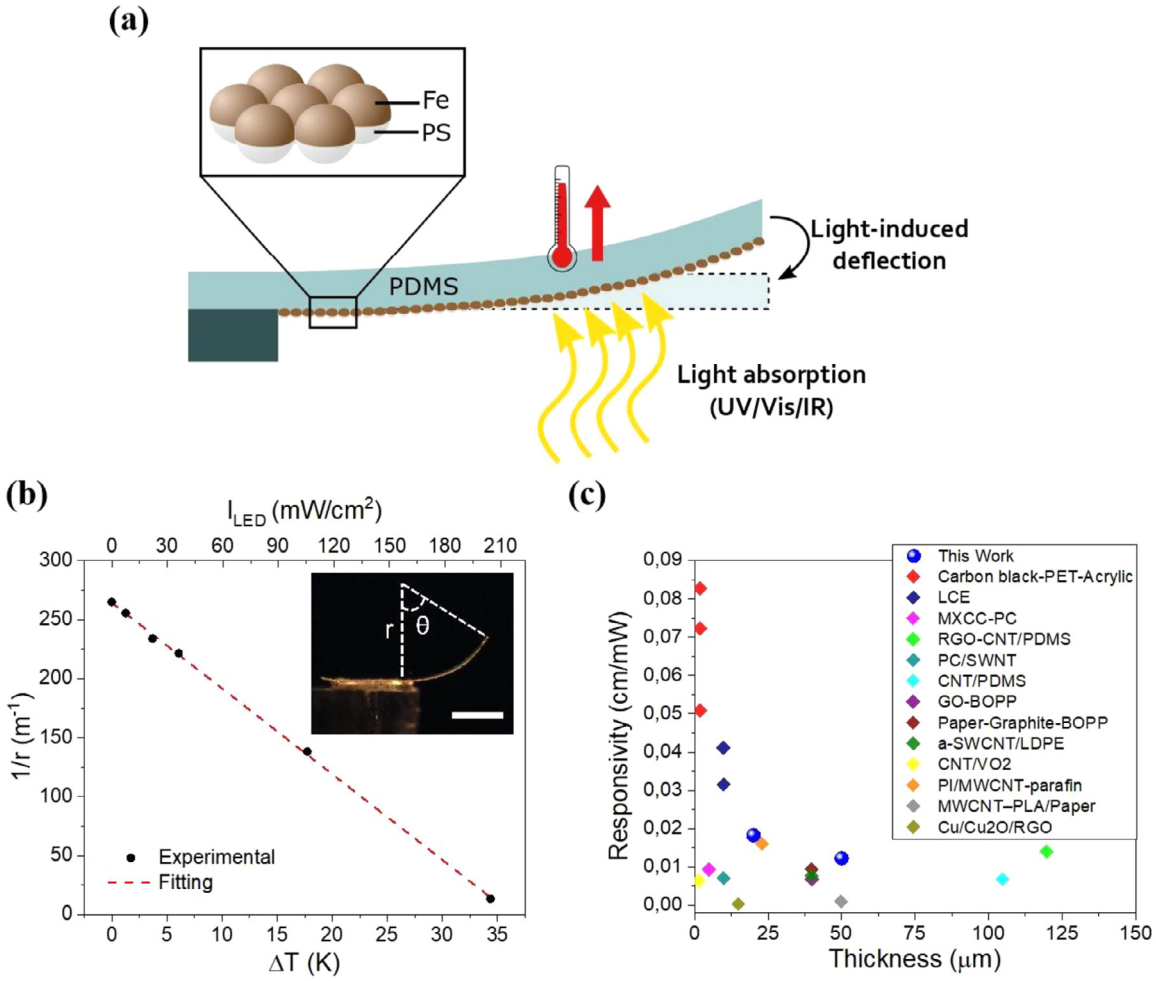

Fig. 4. (a) Schematic of the ultrabroadband opto-mechanical structure principle of operation. (b) Curvature variation in response to light induced temperature changes (bottom axis) and associated white-LED irradiance (top axis). Inset: actual cantilever cross-view picture indicating the curvature radius/angle. Scale-bar = 2 mm. (c) Comparison of the light-to-mechanical conversion efficiency of different photothermal bimorph actuators reported in the literature [21,23,30,31,46–55] (see Table S2 for the description of the different materials).

into 8 segments presenting an initial curvature of 108 ± 6 degrees (Fig. S4), which automatically folded/unfolded depending on the incoming light intensity, thereby opening/closing the inner aperture (Fig. 5a). The biomimetic optomechanical response was characterized by measuring the inner circle diameter of the iris (i.e., the pupil size) as a function of the incoming light irradiance from a white-LED (Fig. 5b). The iris responded linearly to the light irradiance, reaching the nearly closed configuration with 234 mW·cm^{-2}, which corresponds to 1.7-sun intensity [58]. This system was capable of self-adjusting the pupil aperture diameter from 6.9 to 3.8 mm, which is comparable to the standard dynamic range of a natural pupil. The transmitted power through the iris (Fig. 5b, red line) showed a linear self-regulation reaching a relative transmitted power of 56% in the nearly closed configuration, which approximately corresponded to the relative area variation of the pupil. This transmission range can be readily tuned by adjusting the inner hole diameter. To show the ultrabroadband self-regulation of the iris, we analyzed its responsivity, i.e., the variation of the pupil diameter as a function of the incident intensity, for light sources with emission from the visible to the LWIR (Fig. 5c), including the white-LED (Fig. 5b), sunlight, an 808 nm laser (Fig. S5a), and an infrared thermal emitter. Although the wavelength distribution of the white-LED and the natural sunlight are different, their responsivity was nearly equal due to the flat broadband absorption of the Fe/PDMS metamaterial that minimized any wavelength dependence. As observed in Fig. 5c, the iris also responded with similar responsivity to the illumination with monochromatic near-infrared light from the 808 nm laser.

In addition to the visible and NIR, the efficient absorption in the MWIR-LWIR range can also be applied to develop opto-mechanical devices, such as thermal imaging systems [59–61]. Remarkably, the iris also exhibited self-regulation at the MWIR-LWIR range, which was demonstrated by its response to the weak emission from a material heated from room temperature to 120°C (Fig. S6a), in which the blackbody radiation wavelength peaks at 7500 nm. To rule out any contribution from the temperature increase of the air surrounding the iris, two samples of very different emissivity (ε), PDMS (ε = 0.86) and aluminum (ε = 0.04), were heated at the same temperature (Fig. S6b). The iris diameter was reduced a 9% for the PDMS good-emitter, while it barely changed for the Al poor-emitter. Considering the low thermal irradiance at the iris (29.7 mW·cm^{-2}), the responsivity to the thermal IR light was even higher than the other light sources, due to the increased absorption efficiency of the Fe/PDMS metamaterial in the MWIR-LWIR range. Additionally, the temperature increase at the iris upon direct sunlight irradiation was 14.3 °C (Fig. S7), which was enough to actuate the optomechanical system, and reasonably low to be easily insulated and safe for biomedical applications.

Finally, the dynamic response of the biomimetic iris was tested during an on-off cycle using the white-LED (Fig. 5d) and the 808

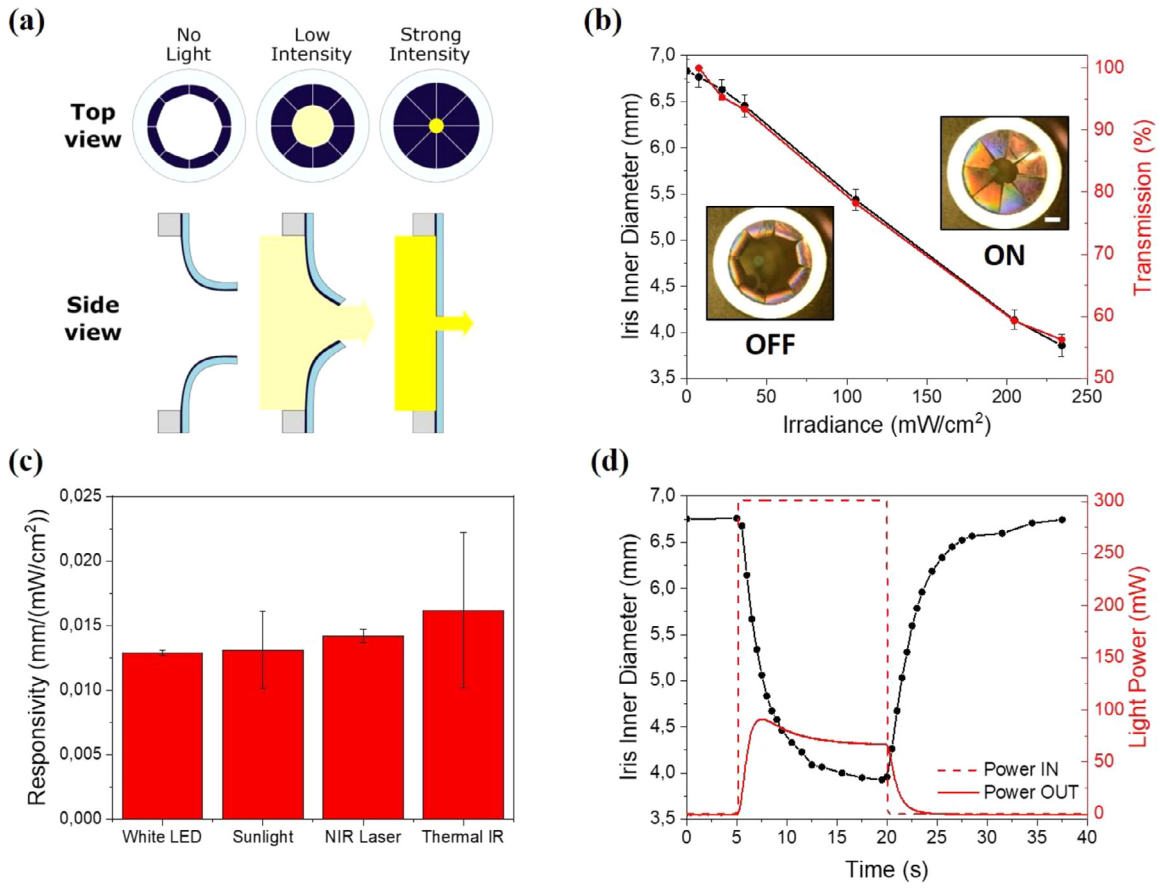

Fig. 5. (a) Schematic of the artificial iris working principle. (b) Diameter of the iris aperture upon white-LED irradiation with increasing irradiance (black squares) and related fraction of the transmitted light power (red circles), together with the actual pictures of the artificial iris with/without white-LED illumination (irradiance 234 mW·cm^{-2}). Scale-bar = 2 mm. (c) Ultrabroadband iris responsivity to different light sources with emission from the visible to the LWIR. (d) Dynamic response of the artificial iris actuated by the white-LED (234 mW·cm^{-2}).

nm laser (Fig. S5b, Video S1). In both cases, the aperture abruptly changed during the initial 4 seconds, followed by a slower thermal stabilization during 10 seconds. Once the light was switched off, the iris returned to the initial position. The transmitted power during the same on-off cycle showed similar dynamic response as the iris diameter. The reaction time was slightly slower than the human iris [62], but it could be matched by optimization of the metamaterial stiffness or geometry. Notably, compared to the previously reported self-regulating artificial iris based on LCE [30], our device presents several advantages, such as a faster and more homogeneous response to small light intensities and a much broader spectral response range. However, it could be of great interest to combine the control on the thermo-mechanical response of LCEs with the ultrabroadband absorber metamaterial presented in this work.

To show the versatility of the Fe/PDMS opto-mechanical metamaterial, we also developed a simple soft mechanic gripper [21,49], consisting of two cantilevers facing each other (Fig. 6a, Video S2). In its relaxed state, the initial bending due to the residual stress configures the gripper in its closed state (step 1). When the gripper is irradiated (step 2), its arms open making it possible to encase the cargo (step 3). As the light irradiation stops, the gripper closes and clutches the cargo, which can be then transported to a different position (steps 4-7). To release the cargo, the gripper can be opened again by light irradiation (steps 8-9). It is worth highlighting the gripper loading capacity, as the cargo weight was remarkably higher (54 mg) than the actuator itself (1 mg). Moreover, the clutching force of the actuator, which depends on the initial stress, can be adjusted by tuning the actuators' length and by controlling residual stress in the fabrication process. On the other hand, the opening strength and velocity can be controlled by the incident light intensity.

Finally, we tested the Fe/PDMS actuator as a remote optically-triggered electrical switch. In this approach, we exploited the optically-controlled bending of the actuator to open/close an electrical circuit and turn off/on a LED (Fig. 6b, Video S3). Since the nanostructured-Fe/PDMS is not conductive, we applied a thin layer of conductive silver paste on the edge of the structure. Even though the actuator's performance was slightly altered due to its weight and stiffness increase, the photo-thermo-mechanical forces were sufficiently strong to bend the free-standing structure and close the electrical circuit. However, in future demonstrations, the incorporation of a conductive pad could be optimized using more sophisticated micropatterning techniques such as inkjet-printing, thus opening the path to light-controlled electrical switches for energy efficiency systems.

4. Conclusion

In summary, we have presented a novel flexible ultrabroadband absorbing nanostructured-Fe/PDMS metamaterial. The optical synergy between the highly damped plasmonic behavior in the nanostructured-Fe layer and the efficient IR absorption in the PDMS enables achieving angle-independent and strong (average 84%) ultrabroadband absorption from the UV to LWIR (300 - 18000 nm), thus overcoming the limitations of typical plasmonic absorbers and multi-layered systems. The angle-independent optical absorption in a large wavelength range translates to an excellent photothermal conversion efficiency. This, combined with the

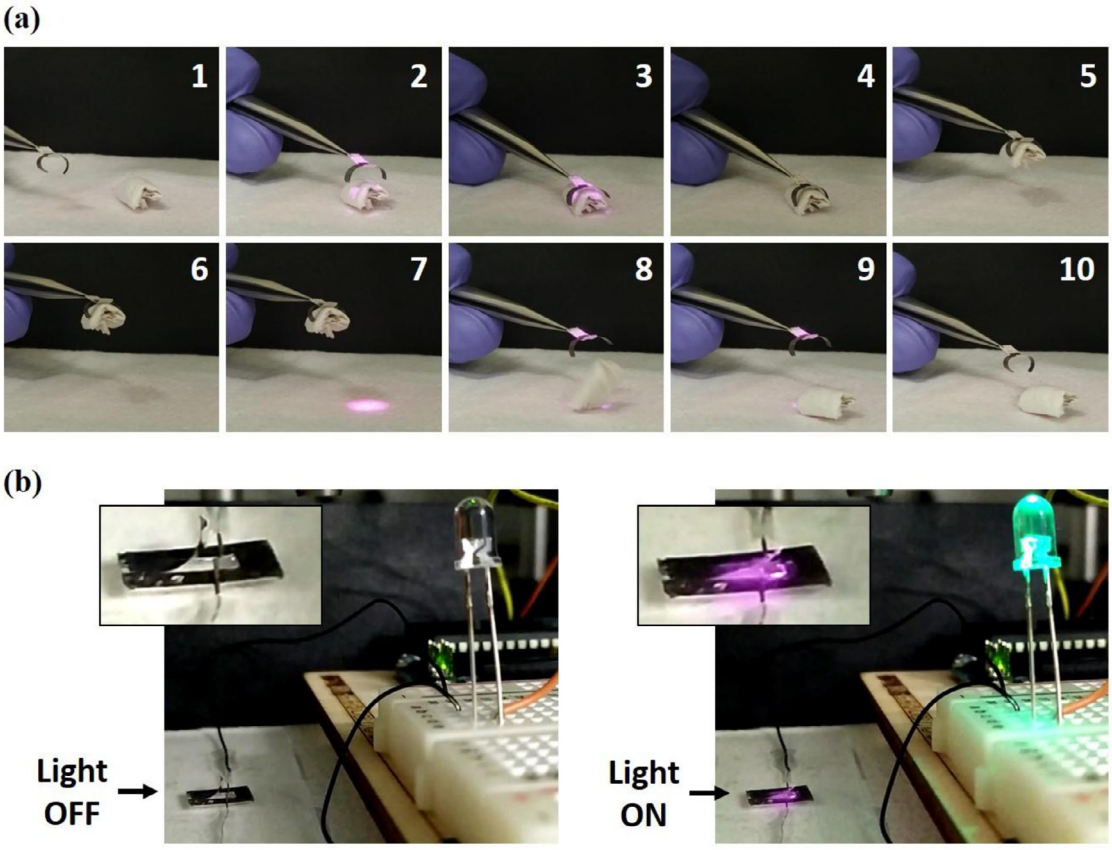

Fig. 6. (a) Pictures of the optically controlled mechanical gripper showing the opening, clutching, transport and release of the cargo. (b) Pictures of the light-triggered electrical switch. The inset pictures show the opto-mechanical actuator that open/closes the electrical circuit and turns on the LED. The incident light (λ = 808 nm) irradiance in (a) and (b) is 242 mW•cm^{-2}.

large thermal expansion mismatch between Fe and PDMS, provides an outstanding opto-mechanical response in suspended structures made of this metamaterial. To exploit these unique features, we demonstrate a self-regulated biomimetic iris capable of responding to an ultrabroadband wavelength range, including natural sunlight and IR thermal radiation. The iris reversibly changes its aperture size following the same dimensions of a natural pupil, and achieves fast, efficient, homogeneous and linear opto-mechanical regulation of the transmitted power. Furthermore, we show the versatile applicability of the metamaterial by developing a light-controlled soft mechanical gripper and a light-triggered electrical switch. Overall, the exceptional photo-thermo-mechanical properties and the versatility and cost-effectiveness of this metamaterial bring new opportunities to develop different types opto-mechanical components, such as dynamic prosthetics, self-regulated and power free light protectors (at any wavelength from UV to LWIR) or light-controlled soft-robots. Furthermore, its ultrabroadband absorption could be exploited in other fields where light collection is crucial, as thermophotovoltaics or photodetection, and the ferromagnetic properties of the iron film could be used to develop multi-stimuli responsive actuators.

Appendix A. Supplementary data

Supplementary data associated with this article can be found, in the online version, at

Data availability

The raw/processed data required to reproduce these findings cannot be shared at this time due to technical or time limitations.

Declaration of Competing Interest

The authors declare that they have no known competing financial interests or personal relationships that could have appeared to influence the work reported in this paper.

CRediT authorship contribution statement

Pau Güell-Grau: Conceptualization, Investigation, Formal analysis, Methodology, Writing – review & editing. **Francesc Pi:** Investigation. **Rosa Villa:** Supervision, Funding acquisition. **Josep Nogués:** Supervision, Funding acquisition, Writing – review & editing. **Mar Alvarez:** Conceptualization, Investigation, Formal analysis, Methodology, Supervision, Funding acquisition, Writing – review & editing. **Borja Sepúlveda:** Conceptualization, Investigation, Formal analysis, Methodology, Supervision, Funding acquisition, Writing – review & editing.

Acknowledgments

We acknowledge funding from Generalitat de Catalunya through the 2017-SGR-292 project. The funding from the Spanish Ministerio de Ciencia, Innovación y Universidades (MICINN) through the MAT2016-77391-R, PID2019-106229RB-I00, PCIN2016-093 (M-ERA-NET), DPI2015-68197-R and DPI2015-72948-EXP projects and Ramon y Cajal Fellowship (RyC2013-14479) is acknowledged. ICN2 is funded by the CERCA programme/Generalitat de Catalunya. The ICN2 is supported by the Severo Ochoa Centres of Excellence programme, funded by the Spanish Research Agency (AEI, grant no. SEV-2017-0706).

Supplementary materials

Supplementary material associated with this article can be found, in the online version, at doi:10.1016/j.apmt.2021.101052.

References

[1] Q. Liu, J. Toudert, T. Li, M. Kramarenko, G. Martínez-Denegri, L. Ciammaruchi, X. Zhan, J. Martorell, Inverse optical cavity design for ultrabroadband light absorption beyond the conventional limit in low-bandgap nonfullerene acceptor–based solar cells, Adv. Energy Mater. 9 (2019) 1900463, doi:10.1002/aenm.201900463.

[2] Y. Wang, T. Sun, T. Paudel, Y. Zhang, Z. Ren, K. Kempa, Metamaterial-plasmonic absorber structure for high efficiency amorphous silicon solar cells, Nano Lett. 12 (2012) 440–445, doi:10.1021/nl203763k.

[3] H. Yuan, X. Liu, F. Afshinmanesh, W. Li, G. Xu, J. Sun, B. Lian, A.G. Curto, G. Ye, Y. Hikita, Z. Shen, S.- C. Zhang, X. Chen, M. Brongersma, H.Y. Hwang, Y. Cui, Polarization-sensitive broadband photodetector using a black phosphorus vertical p–n junction, Nat. Nanotech. 10 (2015) 707–713, doi:10.1038/NNANO.2015.112.

[4] H. Fang, C. Xu, J. Ding, Q. Li, J.- L. Sun, J.- Y. Dai, T.- L. Ren, Q. Yan, Self-powered ultrabroadband photodetector monolithically integrated on a PMN–PT ferroelectric single crystal, ACS Appl. Mater. Interfaces 8 (2016) 32934–32939, doi:10.1021/acsami.6b10305.

[5] J.U. Kim, S. Lee, S.Ji Kang, T. Kim, Materials and design of nanostructured broadband light absorbers for advanced light-to-heat conversion, Nanoscale 10 (2018) 21555–21574, doi:10.1039/C8NR06024J.

[6] P. Yu, L.V. Besteiro, Y. Huang, J. Wu, L. Fu, H.H. Tan, C. Jagadish, G.P. Wiederrecht, A.O. Govorov, Z. Wang, Broadband metamaterial absorbers, Adv. Opt. Mater. 7 (2019) 1800995, doi:10.1002/adom.201800995.

[7] J.R. Hendrickson, S. Vangala, C. Dass, R. Gibson, J. Goldsmith, K. Leedy, D.E. Walker, J.W. Cleary, W. Kim, J. Guo, Coupling of epsilon-near-zero mode to gap Plasmon mode for flat-top wideband perfect light absorption, ACS Photonics 5 (2018) 776–781, doi:10.1021/acsphotonics.7b01491.

[8] Y. Cui, K.H. Fung, J. Xu, H. Ma, Y. Jin, S. He, N.X. Fang, Ultrabroadband light absorption by a sawtooth anisotropic metamaterial slab, Nano Lett. 12 (2012) 1443–1447, doi:10.1021/nl204118h.

[9] W. Li, U. Guler, N. Kinsey, G.V. Naik, A. Boltasseva, J. Guan, V.M. Shalaev, A.V. Kildishev, Refractory plasmonics with titanium nitride: broadband metamaterial absorber, Adv. Mater 26 (2014) 7959–7965, doi:10.1002/adma.201401874.

[10] M. Li, U. Guler, Y. Li, A. Rea, E.K. Tanyi, Y. Kim, M.A. Noginov, Y. Song, A. Boltasseva, V.M. Shalaev, N.A. Kotov, Plasmonic biomimetic nanocomposite with spontaneous subwavelength structuring as broadband absorbers, ACS Energy Lett. 3 (2018) 1578–1583, doi:10.1021/acsenergylett.8b00583.

[11] H. Lin, B.C.P. Sturmberg, K.- T. Lin, Y. Yang, X. Zheng, T.K. Chong, C.M. de Sterke, B. Jia, A 90-nm-thick graphene metamaterial for strong and extremely broadband absorption of unpolarized light, Nat. Photon. 13 (2019) 270, doi:10.1038/s41566-019-0389-3.

[12] Z. Liu, L. Liu, H. Lu, P. Zhan, W. Du, M. Wan, Z. Wang, Ultra-broadband, wide angle absorber utilizing metal insulator multilayers stack with a multi-thickness metal surface texture, Sci. Rep. 7 (2017) 43803, doi:10.1038/s41598-017-04964-3.

[13] H. Zhang, L. Feng, Y. Liang, T. Xu, An ultra-flexible plasmonic metamaterial film for efficient omnidirectional and broadband optical absorption, Nanoscale 11 (2019) 437–443, doi:10.1039/C8NR05276J.

[14] P. Yu, Y. Yao, J. Wu, X. Niu, A.L. Rogach, Z. Wang, Effects of plasmonic metal core -dielectric shell nanoparticles on the broadband light absorption enhancement in thin film solar cells, Sci. Rep. 7 (2017) 7696, doi:10.1038/s41598-017-08077-9.

[15] K. Matsumori, R. Fujimura, Broadband light absorption of an Al semishell-MIM nanostrucure in the UV to near-infrared regions, Opt. Lett. 43 (2018) 2981–2984, doi:10.1364/OL.43.002981.

[16] K. Takatori, T. Okamoto, K. Ishibashi, Surface-Plasmon-induced ultra-broadband light absorber operating in the visible to infrared range, Opt. Express 26 (2018) 1342–1350, doi:10.1364/OE.26.001342.

[17] M.J. Mendes, S. Morawiec, F. Simone, F. Priolo, I. Crupi, Colloidal plasmonic back reflectors for light trapping in solar cells, Nanoscale 6 (2014) 4796–4805, doi:10.1039/C3NR06768H.

[18] Z. Liu, X. Liu, S. Huang, P. Pan, J. Chen, G. Liu, G. Gu, Automatically acquired broadband plasmonic-metamaterial black absorber during the metallic film-formation, ACS Appl. Mater. Interfaces 7 (2015) 4962–4968, doi:10.1021/acsami.5b00056.

[19] D. Liu, F. Zhou, C. Li, T. Zhang, H. Zhang, W. Cai, Y. Li, Black gold: plasmonic colloidosomes with broadband absorption self-assembled from monodispersed gold nanospheres by using a reverse emulsion system, Angew. Chem. Int. Ed. 54 (2015) 9596–9600, doi:10.1002/anie.201503384.

[20] B. Sepúlveda, P.C. Angelomé, L.M. Lechuga, L.M. Liz-Marzán, LSPR-based nanobiosensors, Nano Today 4 (2009) 244–251, doi:10.1016/j.nantod.2009.04.001.

[21] J. Li, R. Zhang, L. Mou, M.J. de Andrade, X. Hu, K. Yu, J. Sun, T. Jia, Y. Dou, H. Chen, S. Fang, D. Qian, Z. Liu, Photothermal bimorph actuators with in-built cooler for light mills, frequency switches, and soft robots, Adv. Funct. Mater. 29 (2019) 1808995, doi:10.1002/adfm.201808995.

[22] H. Lim, T. Park, J. Na, C. Park, B. Kim, E. Kim, Construction of a photothermal Venus flytrap from conductive polymer bimorphs, NPG Asia Mater. 9 (2017) e399, doi:10.1038/am.2017.101.

[23] G. Cai, J.- H. Ciou, Y. Liu, Y. Jiang, P.S. Lee, Leaf-inspired multiresponsive MXene-based actuator for programmable smart devices, Sci. Adv. 5 (2019) eaaw7956, doi:10.1126/sciadv.aaw7956.

[24] M. Pilz da Cunha, Y. Foelen, R.J.H. van Raak, J.N. Murphy, T.A.P. Engels, M.G. Debije, A.P.H.J. Schenning, An untethered magnetic- and light-responsive rotary gripper: shedding light on photoresponsive liquid crystal actuators, Adv. Opt. Mater. 7 (2019) 1801643, doi:10.1002/adom.201801643.

[25] S.M. Mirvakili, I.W. Hunter, Artificial muscles: mechanisms, applications, and challenges, Adv. Mater. 30 (2018) 1704407, doi:10.1002/adma.201704407.

[26] X.- Q. Wang, C.F. Tan, K.H. Chan, X. Lu, L. Zhu, S.- W. Kim, G. W.Ho, In-built thermo-mechanical cooperative feedback mechanism for self-propelled multimodal locomotion and electricity generation, Nat. Commun. 9 (2018) 3438, doi:10.1038/s41467-018-06011-9.

[27] C. Li, Y. Liu, X. Huang, H. Jiang, Direct sun-driven artificial heliotropism for solar energy harvesting based on a photo-thermomechanical liquid-crystal elastomer nanocomposite, Adv. Funct. Mater. 22 (2012) 5166–5174, doi:10.1002/adfm.201202038.

[28] L. Yu, H. Yu, Light-powered tumbler movement of graphene oxide/polymer nanocomposites, ACS Appl. Mater. Interfaces 7 (2015) 3834–3839, doi:10.1021/am508970k.

[29] P. Leeladhar, J. Raturi, P. Singh, Sunlight-driven eco-friendly smart curtain based on infrared responsive graphene oxide-polymer photoactuators, Sci. Rep. 8 (2018) 3687, doi:10.1038/s41598-018-21871-3.

[30] H. Zeng, O.M. Wani, P. Wasylczyk, R. Kaczmarek, A. Priimagi, Self-regulating iris based on light-actuated liquid crystal elastomer, Adv. Mater. 29 (2017) 1701814, doi:10.1002/adma.201701814.

[31] X. Zhang, Z. Yu, C. Wang, D. Zarrouk, J.- W.T. Seo, J.C. Cheng, A.D. Buchan, K. Takei, Y. Zhao, J.W. Ager, J. Zhang, M. Hettick, M.C. Hersam, A.P. Pisano, R.S. Fearing, A. Javey, Photoactuators and motors based on carbon nanotubes with selective chirality distributions, Nat. Commun. 5 (2014) 2983, doi:10.1038/ncomms3983.

[32] Z. Li, A. Lopez-Ortega, A. Aranda-Ramos, J.L. Tajada, J. Sort, C. Nogues, P. Vavassori, J. Nogues, B. Sepulveda, Simultaneous local heating/thermometry based on plasmonic magnetochromic nanoheaters, Small 14 (2018) 1800868, doi:10.1002/smll.201800868.

[33] Z. Li, A. Aranda-Ramos, P. Güell-Grau, J.L. Tajada, L. Pou-Macayo, S. Lope Piedrafita, F. Pi, A.G. Roca, M.D. Baró, J. Sort, C. Nogués, J. Nogués, B. Sepúlveda, Magnetically amplified photothermal therapies and multimodal imaging with magneto-plasmonic nanodomes, Appl. Mater. Today 12 (2018) 430–440, doi:10.1016/j.apmt.2018.07.008.

[34] N.E. Stankova, P.A. Atanasov, R.G. Nikov, R.G. Nikov, N.N. Nedyalkov, T.R. Stoyanchov, N. Fukata, K.N. Kolev, E.I. Valova, J.S. Georgieva, S.A. Armyanov, Optical properties of polydimethylsiloxane (PDMS) during nanosecond laser processing, Appl. Surf. Sci. 374 (2016) 96–103, doi:10.1016/j.apsusc.2015.10.016.

[35] K. Aydin, V.E. Ferry, R.M. Briggs, H.A. Atwater, Broadband polarization-independent resonant light absorption using ultrathin plasmonic super absorbers, Nat. Commun. 2 (2011) 517, doi:10.1038/ncomms1528.

[36] K. Bae, G. Kang, S.K. Cho, W. Park, K. Kim, W.J. Padilla, Flexible thin-film black gold membranes with ultrabroadband plasmonic nanofocusing for efficient solar vapour generation, Nat. Commun. 6 (2015) 10103, doi:10.1038/ncomms10103.

[37] Y. Hui, J.S. Gomez-Diaz, Z. Qian, A. Alù, M. Rinaldi, Plasmonic piezoelectric nanomechanical resonator for spectrally selective infrared sensing, Nat. Commun. 7 (2016) 11249, doi:10.1038/ncomms11249.

[38] T. Ji, L. Peng, Y. Zhu, F. Yang, Y. Cui, X. Wu, L. Liu, S. He, F. Zhu, Y. Hao, Plasmonic broadband absorber by stacking multiple metallic nanoparticle layers, Appl. Phys. Lett. 106 (2015) 161107, doi:10.1063/1.4919106.

[39] P. Zhu, L.J. Guo, High performance broadband absorber in the visible band by engineered dispersion and geometry of a metal-dielectric-metal stack, Appl. Phys. Lett. 101 (2012) 241116, doi:10.1063/1.4771994.

[40] M.K. Hedayati, A.U. Zillohu, T. Strunskus, F. Faupel, M. Elbahri, Plasmonic tunable metamaterial absorber as ultraviolet protection film, Appl. Phys. Lett. 104 (2014) 041103, doi:10.1063/1.4863202.

[41] W. Guo, Y. Liu, T. Han, Ultra-broadband infrared metasurface absorber, Opt. Express 24 (2016) 20586–20592, doi:10.1364/OE.24.020586.

[42] L. Lei, S. Li, H. Huang, K. Tao, P. Xu, Ultra-broadband absorber from visible to near-infrared using plasmonic metamaterial, Opt. Express 26 (2018) 5686–5693, doi:10.1364/OE.26.005686.

[43] X. Tian, Z.- Y. Li, Visible-near infrared ultra-broadband polarization-independent metamaterial perfect absorber involving phase-change materials, Photon. Res. 4 (2016) 146–152, doi:10.1364/PRJ.4.000146.

[44] E. Popov, D. Maystre, R.C. McPhedran, M. Nevière, M.C. Hutley, G.H. Derrick, Total absorption of unpolarized light by crossed gratings, Opt. Express 16 (2008) 6146–6155, doi:10.1364/OE.16.006146.

[45] A. Mata, A.J. Fleischman, S. Roy, Characterization of polydimethylsiloxane (PDMS) properties for biomedical micro/nanosystems, Biomed. Microdevices 7 (2005) 281–293, doi:10.1007/s10544-005-6070-2.

[46] Y. Hu, G. Wu, T. Lan, J. Zhao, Y. Liu, W. Chen, A graphene-based bimorph structure for design of high performance photoactuators, Adv. Mater. 27 (2015) 7867–7873, doi:10.1002/adma.201502777.

[47] J. Mu, C. Hou, H. Wang, Y. Li, Q. Zhang, M. Zhu, Origami-inspired active graphene-based paper for programmable instant self-folding walking devices, Sci. Adv. 1 (2015) e1500533, doi:10.1126/sciadv.1500533.

[48] Y. Hu, J. Liu, L. Chang, L. Yang, A. Xu, K. Qi, P. Lu, G. Wu, W. Chen, Y. Wu, Electrically and sunlight-driven actuator with versatile biomimetic motions based on rolled carbon nanotube bilayer composite, Adv. Funct. Mater. 27 (2017) 1704388, doi:10.1002/adfm.201704388.
[49] L. Chen, M. Weng, P. Zhou, L. Zhang, Z. Huang, W. Zhang, Multi-responsive actuators based on a graphene oxide composite: intelligent robot and bioinspired applications, Nanoscale 9 (2017) 9825–9833, doi:10.1039/C7NR01913K.
[50] M. Weng, P. Zhou, L. Chen, L. Zhang, W. Zhang, Z. Huang, C. Liu, S. Fan, Multiresponsive bidirectional bending actuators fabricated by a pencil-on-paper method, Adv. Funct. Mater. 26 (2016) 7244–7253, doi:10.1002/adfm.201602772.
[51] L. Li, J. Meng, C. Hou, Q. Zhang, Y. Li, H. Yu, H. Wang, Dual-mechanism and multimotion soft actuators based on commercial plastic film, ACS Appl. Mater. Interfaces 10 (2018) 15122–15128, doi:10.1021/acsami.8b00396.
[52] H. Ma, J. Hou, X. Wang, J. Zhang, Z. Yuan, L. Xiao, Y. Wei, S. Fan, K. Jiang, K. Liu, Flexible, all-inorganic actuators based on vanadium dioxide and carbon nanotube bimorphs, Nano Lett. 17 (2017) 421–428, doi:10.1021/acs.nanolett.6b04393.
[53] P. Zhou, L. Chen, L. Yao, M. Weng, W. Zhang, Humidity- and light-driven actuators based on carbon nanotube-coated paper and polymer composite, Nanoscale 10 (2018) 8422–8427, doi:10.1039/C7NR09580E.
[54] D. Hua, X. Zhang, Z. Ji, C. Yan, B. Yu, Y. Li, X. Wang, F. Zhou, 3D printing of shape changing composites for constructing flexible paper-based photothermal bilayer actuators, J. Mater. Chem. C 6 (2018) 2123–2131, doi:10.1039/C7TC05710E.
[55] J. Meng, J. Mu, C. Hou, Q. Zhang, Y. Li, H. Wang, A flexible metallic actuator using reduced graphene oxide as a multifunctional component, Nanoscale 9 (2017) 12963–12968, doi:10.1039/C7NR03028B.
[56] K.R. Koch, L.M. Heindl, C. Cursiefen, H.- R. Koch, Artificial iris devices: benefits, limitations, and management of complications, J. Cataract Refract. Surg. 40 (2014) 376–382, doi:10.1016/j.jcrs.2013.08.051.
[57] S. Thainimit, L.A. Alexandre, V.M.N. de Almeida, Iris surface deformation and normalization, in: Proceedings of the 13th International Symposium on Communications and Information Technologies, 2013, pp. 501–506, doi:10.1109/ISCIT.2013.6645910. IEEE.
[58] C.A. Gueymard, The sun's total and spectral irradiance for solar energy applications and solar radiation models, Sol. Energy 76 (2004) 423–453, doi:10.1016/j.solener.2003.08.039.
[59] R. Amantea, C.M. Knoedler, F.P. Pantuso, V. Patel, D.J. Sauer, J.R. Tower, Uncooled IR imager with 5-mK NEDT, Proc. SPIE 3061 (1997) 210–222, doi:10.1117/12.280340.
[60] R. Amantea, L.A. Goodman, F.P. Pantuso, D.J. Sauer, M. Varghese, T.S. Villani, L.K. White, Progress toward an uncooled IR imager with 5-mK NETD, Proc. SPIE 3436 (1998) 647–659, doi:10.1117/12.328065.
[61] J. Zhao, High sensitivity photomechanical MW-LWIR imaging using an uncooled MEMS microcantilever array and optical readout, Proc. SPIE 5783 (2005) 506-513, doi:10.1117/12.606485.
[62] H.S. Gradle, W. Ackerman, The reaction time of the normal pupil: second communication, J. Am. Med. Assoc. 99 (1932) 1334–1336, doi:10.1001/jama.1932.02740680030008.